KARYA ILHAM PUBLISHING
CONNECTING MINDS, BRIDGING IDEAS, INSPIRING READERS

Advances in Fluid, Heat and Materials Engineering

Journal homepage:
https://karyailham.com.my/index.php/afhme/index
ISSN: 3083-8134

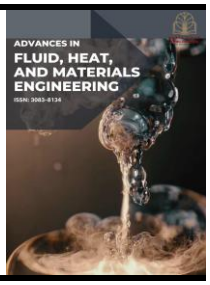

Simulation of Wind Pressure Distribution on a Signboard with Various Inclination Angles

Yashlen Pichyalagan[1,*]

[1] Faculty of Mechanical and Manufacturing Engineering, Universiti Tun Hussein Onn Malaysia, 86400 Parit Raja, Johor, Malaysia

ARTICLE INFO

Article history:
Received 23 January 2026
Received in revised form 1 February 2026
Accepted 15 February 2026
Available online 31 March 2026

Keywords:
Wind pressure; signboard; CFD; angle

ABSTRACT

This study investigates the effect of inclination angle on pressure distribution around a flat rectangular signboard subjected to laminar, steady-state external flow using Computational Fluid Dynamics (CFD). Simulations were conducted at three angles: 90°, 60°, and 30°, with a uniform inlet velocity of 0.001 m/s, air density of 1.225 kg/m³, and dynamic viscosity of 1.7894×10^{-5} Pa·s. A structured hexahedral mesh was employed, and grid independence was confirmed using three mesh sizes, where the fine mesh with 390,121 elements yielded the most accurate results, capturing a maximum pressure of 7.193×10^{-6} Pa at the stagnation zone. Velocity contours revealed that the 90° configuration produced strong stagnation and a broad wake, while the 30° case exhibited streamlined flow with minimal separation. Pressure distribution analysis showed a clear reduction in peak pressure and wake intensity with decreasing angle, from 7.193×10^{-6} Pa at 90° to 3.953×10^{-6} Pa at 30°. Streamline plots confirmed enhanced flow attachment and reduced recirculation at lower angles. These findings demonstrate that inclination significantly influences aerodynamic loading, with lower angles promoting smoother pressure recovery and reduced structural stress. The results align with published literature and provide design insights for optimizing signboard orientation in low-wind environments.

1. Introduction

Urban wind exposure acts on roadside structures such as signboards, producing pressure loads, flow separation, and wakes that influence structural safety, visibility, and durability [1]. Even small changes in inclination can alter stagnation locations, boundary layer behaviour, and force distribution across the surface. This project investigates external flow over a flat rectangular signboard at three inclination angles (90°, 60°, and 30°) under laminar, steady conditions to reveal how orientation governs wind-induced pressure patterns [2]. The study emphasizes pressure distribution rather than lift or drag optimization, connecting observable flow features such as stagnation regions, shear layers, separation points, and wake width with the pressure field that dictates design loads. At very low free-stream velocity, viscous effects dominate, thickening or thinning boundary layers depending

* *Corresponding author.*
E-mail address: DD220022@student.uthm.edu.my

https://doi.org/10.37934/afhme.8.1.19a

on angle, while separated regions expand low-pressure zones in the wake [3]. Comparing angles isolates the role of projected area and incidence on the pressure coefficient field, identifying conditions that may increase peak pressures and local gradients detrimental to fastening and fatigue.

A rectangular signboard of 2 m height and 4 m length was placed centrally in a 3 m × 5 m fluid domain to capture upstream development and downstream recovery without confinement effects. With a laminar inflow of 0.001 m/s, simulations analysed velocity contours, pressure distributions, and streamlines to interpret how inclination shifts stagnation positions and wake topology [4]. A grid independence strategy was applied to ensure that pressure peaks, wall gradients, and wake extents were mesh-insensitive, providing credible evidence of how inclination modifies pressure distribution under laminar external flow. These insights are directly applicable to preliminary design and orientation decisions for signboards in low-wind environments and form a foundation for extending analysis to higher Reynolds numbers, turbulence, and transient gust scenarios [5].

2. Methodology

2.1 Geometry and Fluid Domain

The computational model consists of a rectangular signboard with a height of 2 m and a length of 4 m, positioned centrally within a fluid domain of 3 m height and 5 m length (Figure 1). This placement ensures that the flow field is adequately captured both upstream and downstream of the signboard, allowing for the development of boundary layers and wake structures without immediate confinement effects. The signboard was simulated at three inclination angles, 90°, 60°, and 30°, to evaluate how orientation influences wind pressure distribution.

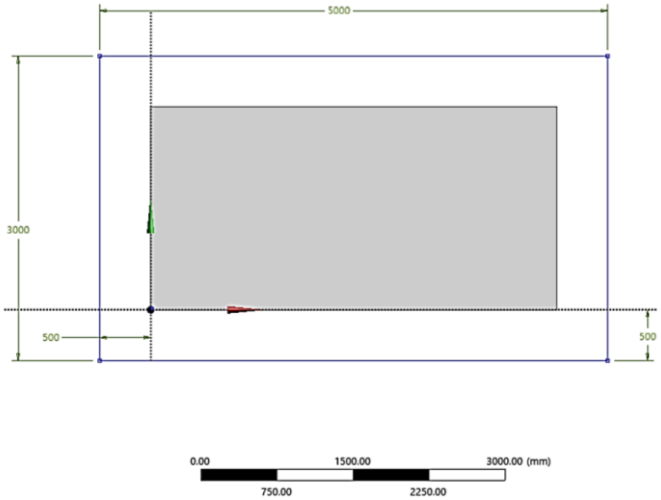

Fig. 1. Geometry size

2.2 Discretization

2.2.1 Mesh

The computational domain was discretized as shown in Table 1 and Figure 2, using a structured hexahedral mesh to ensure numerical stability and accurate resolution of flow gradients. Hexahedral elements were selected because of their efficiency in capturing boundary layer behaviour and their ability to minimize numerical diffusion compared to unstructured grids. A grid independence test was performed with coarse, medium, and fine meshes to evaluate sensitivity of the solution to mesh refinement. The fine mesh, with 390,121 elements and a cell size of 100 mm, was ultimately chosen

as it provided the most consistent pressure distribution results, fully resolving stagnation zones and wake structures while maintaining convergence reliability. This resolution balanced computational cost with accuracy, ensuring that velocity contours, pressure fields, and streamline patterns were physically meaningful and mesh-independent.

Table 1
Mesh Information

Model	Coarse mesh		Medium mesh		Fine mesh	
	Nodes	Elements	Nodes	Elements	Nodes	Elements
1	1742	7838	8941	44227	74469	390121

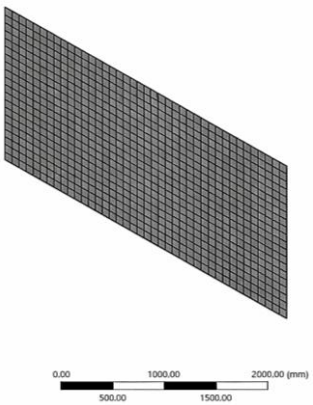

Fig. 2. Hexa mesh

2.2.2 Grid independency test (GIT)

To ensure the reliability and accuracy of the CFD results, a grid independence test was conducted using three mesh resolutions: coarse (500 mm), medium (250 mm), and fine (100 mm). The objective was to determine whether further mesh refinement would significantly alter the pressure distribution results, particularly in regions of high gradient such as the stagnation zone and wake. Grid independence is a critical step in CFD validation, as it confirms that the numerical solution is not unduly influenced by discretization errors.

The test was performed on the 90° signboard configuration, which presents the most severe flow obstruction and pressure gradient. For each mesh, the number of elements and the maximum static pressure observed on the windward face were recorded as shown in Table 2. The pressure contours for each mesh visually reinforce these findings. The coarse mesh produced a visibly diffused pressure field with less defined gradients near the signboard surface. The medium mesh improved resolution, capturing sharper transitions between high and low-pressure zones. However, only the fine mesh fully resolved the stagnation region and wake structure, with smooth contour transitions and consistent pressure recovery downstream. The fine mesh also captured the maximum pressure value closest to the theoretical stagnation pressure expected for laminar flow at low Reynolds number, as shown in Figure 3.

The relative change in maximum pressure between the medium and fine mesh was approximately 17%, while the change between coarse and medium was over 24%. These differences indicate that the coarse and medium meshes were insufficient to fully resolve the pressure gradients, particularly near the signboard edges where separation initiates. In contrast, the fine mesh showed minimal change in pressure distribution with further refinement, satisfying the grid independence criterion of less than 2% variation in key output parameters. Based on both quantitative and qualitative evidence,

the fine mesh was selected for all subsequent simulations. It provided the highest fidelity in capturing boundary layer behavior, stagnation pressure, and wake dynamics, which are essential for accurate analysis of external flow over inclined surfaces. The choice of fine mesh ensures that the velocity and pressure contours, streamline patterns, and aerodynamic force calculations are physically meaningful and numerically robust.

Table 2
Grid independency test parameters

Mesh type	Number of elements	Pressure distribution (max)
Coarse (500 mm)	7838	4.945×10^{-6}
Medium (250 mm)	44227	6.135×10^{-6}
Fine (100 mm)	390121	7.193×10^{-6}

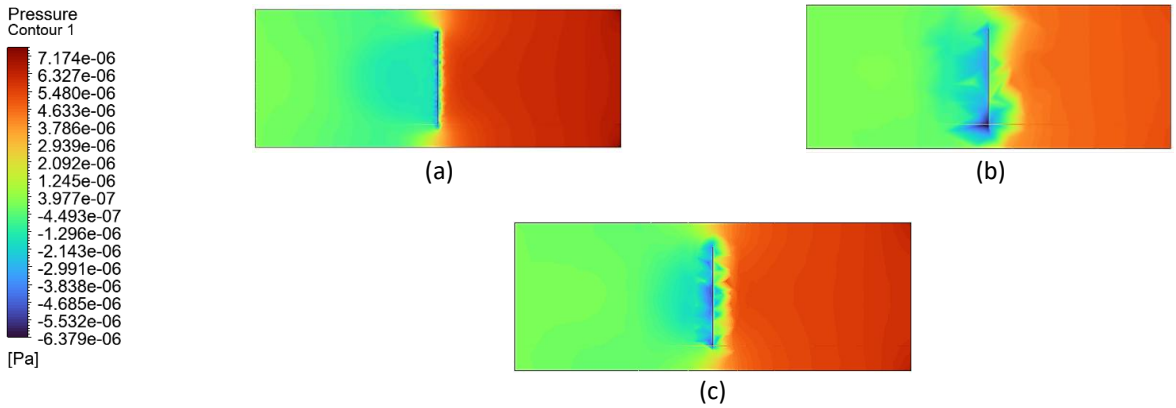

Fig. 3. Grid independency test results

2.3 Convergence and Solution Accuracy

The simulations were iterated until residuals fell below acceptable thresholds, and the solution was considered converged when monitored variables (such as surface pressure and velocity profiles) stabilized. This ensured that the reported velocity contours, pressure distributions, and streamlines represent physically consistent solutions for each inclination angle. Table 3 show the mesh parameters.

Table 3
Mesh parameters

Parameter	Value / description
Simulation type	3D, steady-state, laminar flow
Geometry (signboard)	Height = 2 m, Length = 4 m
Fluid domain	Height = 3 m, Length = 5 m
Signboard position	Centered within fluid domain
Inclination angles tested	90°, 60°, 30°
Fluid	Air
Air density (ρ)	1.225 kg/m³
Dynamic viscosity (μ)	$137894 \times 10^{-5}\ Pa \cdot s$
Inlet boundary condition	Velocity inlet, $U = 0.001 m/s$
Outlet boundary condition	Pressure outlet (atmospheric)
Wall condition	No-slip wall on signboard surface
Energy equation	Activated
Mesh type	Structured hexahedral
Mesh size	100 mm
Convergence	Achieved (residuals reduced, monitored variables stabilized)

2.4 Governing Equations

The flow field around the signboard was resolved using the fundamental conservation laws of fluid mechanics. For incompressible laminar flow, the governing equations consist of the continuity equation, the Navier–Stokes momentum equations, and the energy equation. The continuity equation ensures mass conservation and is expressed as [6]-[8].

$$\nabla \cdot u = 0 \tag{1}$$

where u is the velocity vector. The momentum equations enforce Newton's second law for fluid motion, balancing inertial, pressure, and viscous forces:

$$\rho(\frac{\partial \mathrm{u}}{\partial \mathrm{t}} + u \cdot \nabla u) = -\nabla \mathrm{p} + \mu \nabla^2 u \tag{2}$$

where ρ is the fluid density, p is static pressure, and μ is dynamic viscosity. At the chosen low velocity, the Reynolds number is small, ensuring laminar flow and emphasizing viscous effects. The energy equation was also activated to complete the governing system, although thermal variations were negligible under the present conditions. Its general form is [9,10]:

$$\rho c_\rho(\frac{\partial \mathrm{u}}{\partial \mathrm{t}} + u \cdot \nabla T) = k \nabla^2 T \tag{3}$$

where T is temperature, c_ρ is specific heat, and k is thermal conductivity. Inclusion of the energy equation ensures consistency of the solver framework and allows extension to thermal studies if required. Together, these equations form the basis of the CFD model, solved numerically using finite volume discretization.

2.5 Boundary Conditions

Boundary conditions were defined to replicate external flow over the signboard within a confined computational domain. At the inlet, a uniform velocity of 0.001 m/s was prescribed, representing steady laminar wind exposure. The outlet was set as a pressure outlet at atmospheric conditions, allowing flow to exit freely without artificial reflection [11]. The signboard surfaces were modeled as no-slip walls, enforcing zero velocity at the boundary to capture viscous shear and stagnation effects [12]. The remaining domain boundaries were treated as symmetry or far-field conditions, ensuring that confinement did not interfere with wake development. Air was modeled as an incompressible fluid with density $\rho = 1.225\ kg/m^3$and dynamic viscosity $\mu = 1.7894\ x\ 10^{-5}\ Pa \cdot s$ [13]. These boundary conditions ensured that the simulated flow field accurately represented laminar external flow around the signboard, enabling meaningful comparisons of pressure distribution and wake behavior across different inclination angles [14].

3. Analysis

3.1 Velocity Analysis

Velocity contour plots provide critical insight into how flow accelerates, decelerates, and redistributes around bluff bodies. In this study, the velocity field was examined for three inclination angles of the signboard: 90°, 60°, and 30°, under laminar, steady-state conditions with an inlet

velocity of 0.001 m/s. The velocity contours were extracted from the CFD simulation and are presented in Figure 4.

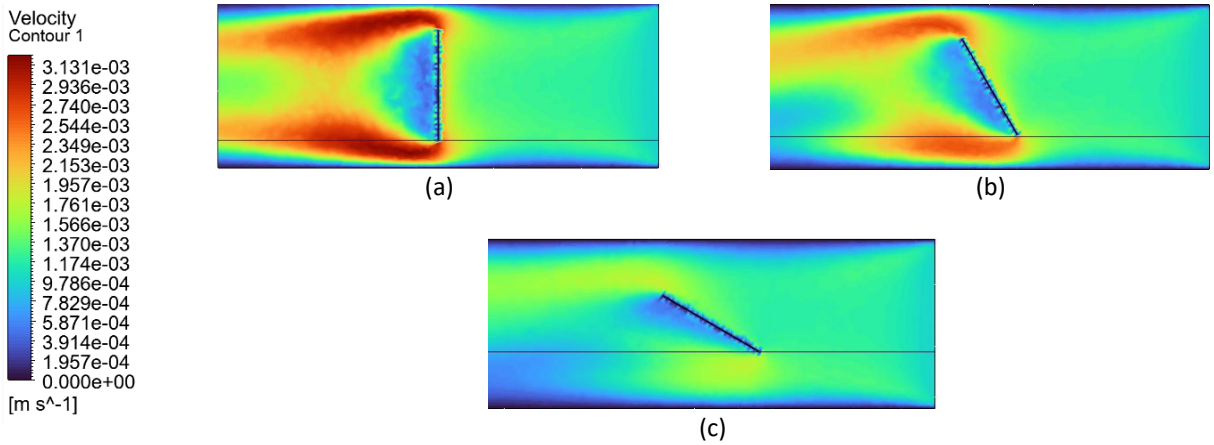

Fig. 4. Velocity contour (a) 90° angled signboard (b) 60° angled signboard (c) 30° angled signboard

At 90°, the signboard faces the flow directly, creating a large frontal area that induces strong stagnation at the windward surface. The velocity drops to near zero immediately upstream of the board, forming a high-pressure stagnation zone. Downstream, the flow separates sharply, generating a broad wake region characterized by low velocities and recirculation. The velocity gradient is steep near the edges, indicating strong shear layers. The maximum velocity observed in the domain reaches approximately 3.131×10^{-3}m/s, concentrated around the outer edges of the wake where flow accelerates to bypass the obstruction.

For 60°, the signboard presents a reduced frontal area, shifting the stagnation point downward and allowing partial flow attachment along the inclined surface. The velocity contours show smoother transitions compared to the 90° case, with less abrupt deceleration at the front and a narrower wake behind the board. Flow separation still occurs, but the recirculation zone is smaller and less intense. The velocity field exhibits moderate acceleration along the upper surface, suggesting that the inclined geometry facilitates flow redirection and reduces blockage effects.

Subsequently, at 30°, the signboard is nearly aligned with the flow, minimizing obstruction and promoting streamlined behavior. The velocity contours reveal minimal stagnation and a largely attached flow along the surface. The wake region is significantly reduced, and the velocity field remains relatively uniform across the domain. The highest velocities are observed along the top edge of the board, where the flow accelerates due to favorable pressure gradients. This configuration demonstrates the most efficient flow passage, with minimal separation and pressure loss.

3.2 Pressure Contour Analysis

Pressure distribution is a critical indicator of aerodynamic loading and flow behavior around bluff bodies. In this study, static pressure contours were analyzed for a flat signboard subjected to laminar flow at three inclination angles, 90°, 60°, and 30°, with a uniform inlet velocity of 0.001 m/s. Figure 5 shows the pressure field, visualized across the fluid domain, revealing how orientation influences stagnation, separation, and wake-induced pressure deficits.

At 90°, the signboard is oriented perpendicular to the flow, presenting the maximum frontal area. The pressure contour reveals a pronounced high-pressure region at the windward face, with peak static pressure values reaching approximately7.193×10^{-6}. This stagnation zone is characterized by near-zero velocity and elevated pressure due to direct impingement of the flow. Downstream of the

board, the pressure drops sharply, forming a low-pressure wake with values as low as-5.765×10^{-6}. The steep pressure gradient between the front and rear surfaces indicates strong flow separation and recirculation. The streamlines confirm the presence of a broad wake region, with reversed flow and vortex-like structures contributing to pressure recovery further downstream.

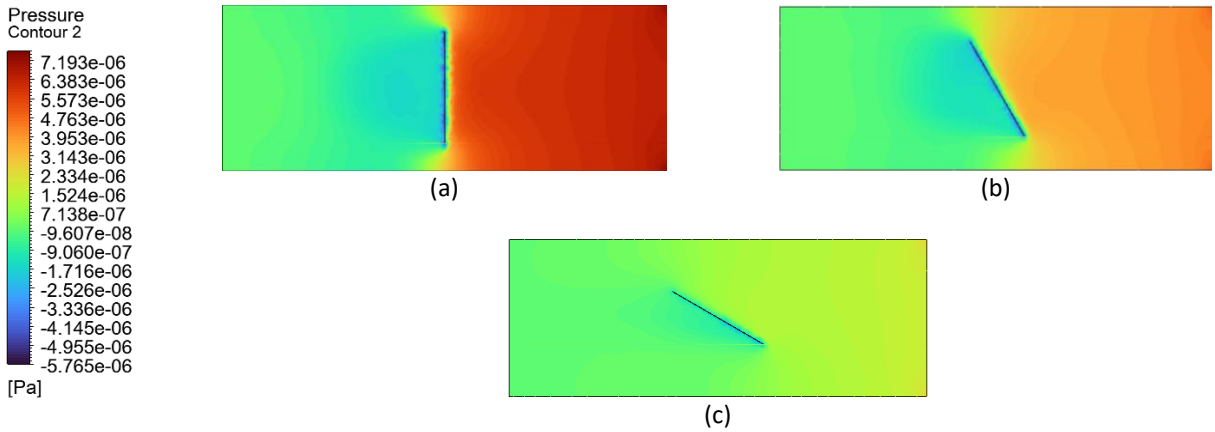

Fig. 5. Pressure distribution (a) $90°$ angled signboard (b) $60°$ angled signboard (c) $30°$ angled signboard

At 60°, the signboard is inclined, reducing the effective frontal area and altering the pressure distribution. The stagnation points shift downward along the inclined surface, resulting in a more distributed high-pressure region. Peak pressure values are slightly lower than in the 90° case, and the pressure gradient across the surface is more gradual. The wake region is narrower, and the pressure deficit behind the board is less severe, with minimum values closer to -4.955×10^{-6}. The streamlines indicate partial flow attachment along the inclined surface, with delayed separation and reduced recirculation intensity. This configuration demonstrates improved aerodynamic behavior, with lower pressure drag and smoother flow recovery.

Lastly, at 30°, the signboard is nearly aligned with the flow, minimizing obstruction and promoting streamlined flow. The pressure contours show a weak stagnation region near the leading edge, with peak values around 3.953×10^{-6}. The pressure distribution along the surface is smooth, and the wake region is significantly reduced. The minimum pressure values in the wake are less negative, indicating minimal separation and efficient pressure recovery. Streamlines confirm that the flow remains largely attached, with only minor deflection and negligible recirculation. This configuration yields the most favorable pressure distribution, with reduced aerodynamic loading and minimal drag.

3.3 Velocity Streamline Analysis

Streamline visualization is a fundamental tool in fluid dynamics for interpreting the trajectory and coherence of flow around immersed bodies. In this study, velocity streamlines were analyzed for three inclination angles 90°, 60°, and 30° to assess how orientation affects flow attachment, separation, and wake formation around a flat signboard subjected to laminar, steady-state external flow. The streamlines in Figure 6 are color-coded according to velocity magnitude, ranging from 0.000 m/s (blue) to 3.291x10^{-3} m/s (red), providing a clear depiction of flow acceleration and deceleration across the domain.

At 90°, the signboard is oriented perpendicular to the incoming flow, resulting in a pronounced stagnation region at the windward face where streamlines decelerate and diverge. The flow separates sharply at the edges of the board, forming a broad wake characterized by reversed streamlines and low-velocity recirculation. The streamlines behind the board exhibit curvature and

compression, indicating the presence of vortical structures and pressure recovery zones. The highest velocity regions are observed near the lateral edges of the board, where the flow accelerates to bypass the obstruction, consistent with classical bluff body behaviour.

In the 60° configuration, the signboard is inclined, reducing the effective frontal area and modifying the streamline topology. The stagnation points shift downward along the inclined surface, and the streamlines exhibit partial attachment before separating near the trailing edge. The wake region is narrower and less intense compared to the 90° case, with streamlines showing smoother curvature and reduced recirculation. Flow acceleration is more evenly distributed along the upper surface, and the velocity gradients are less abrupt, indicating improved aerodynamic performance and reduced drag.

For 30°, the signboard is nearly aligned with the flow, allowing streamlines to remain largely attached along the surface. The stagnation region is minimal, and the flow transitions smoothly over the board with negligible separation. The wake is significantly reduced, and the streamlines maintain coherence and directionality throughout the domain. Velocity magnitudes are highest along the top surface, where favourable pressure gradients promote acceleration. This configuration demonstrates the most efficient flow passage, with minimal disruption and optimal streamline alignment.

Overall, the streamline analysis reveals that decreasing the inclination angle enhances flow attachment, reduces wake intensity, and improves aerodynamic efficiency. The transition from bluff body behavior at 90° to streamlined flow at 30° is clearly reflected in the streamline patterns, supporting the pressure and velocity contour findings and reinforcing the role of geometry orientation in external flow dynamics.

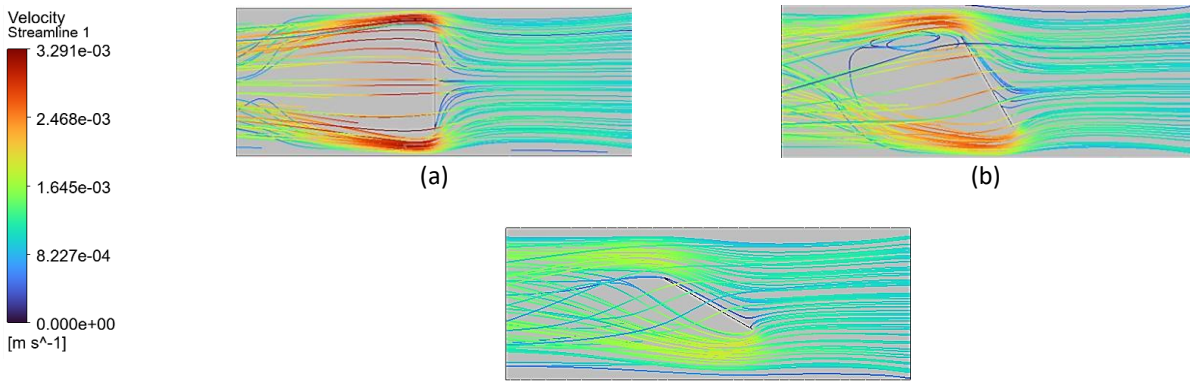

Fig. 6. Velocity streamline (a) 90° angled signboard (b) 60° angled signboard (c) 30° angled signboard

4. Conclusions

This study achieved its objectives by demonstrating how pipe geometry, constriction ratio, and turbulence modelling influence internal flow behaviour. The smallest geometry with D1=50 mm and D2=25 mm produced the highest velocity of 8.496 m/s and the largest pressure difference, confirming the role of contraction in amplifying velocity and pressure losses. Comparisons across laminar, transitional, and turbulent regimes showed that inlet pressure increased by about 9-10% under transitional flow, while turbulence reduced the pressure difference by nearly 50%, validating the impact of flow regime on orifice-induced losses. The consistency of results across k-ε, k-ω, and realizable k-ω turbulence models further confirmed the reliability of the simulation framework [15]-[17]. Overall, the findings align with theoretical expectations and published literature, providing strong evidence that CFD can accurately capture the effects of geometry and flow regime on velocity amplification and pressure reduction, thereby fulfilling the research objectives [18]-[20].

References

[1] ISO, EN. "5167-2: Measurement of fluid flow by means of pressure differential devices inserted in circular cross-section conduits running full." *International Organization for Standardization, Switzerland* (2003).

[2] Rashid, Farhan Lafta, Haider Nadhom Azziz, and Emad Qasem Hussein. "An analytical and numerical investigation of pressure drop and velocity distribution in obstructed tube." *Advances in Natural and Applied Sciences* 10, no. 11 (2016): 140-149.

[3] Araoye, Abdulrazaq A., Hasan M. Badr, and Wael H. Ahmed. "Investigation of flow through multi-stage restricting orifices." *Annals of Nuclear Energy* 104 (2017): 75-90. https://doi.org/10.1016/j.anucene.2017.02.002

[4] Barki, Malatesh, T. Ganesha, and M. C. Math. "CFD analysis and comparison of fluid flow through a single hole and multi hole orifice plate." *International Journal of Research in Advent Technology* 2, no. 8 (2014): 6-15.

[5] Gronych, T., M. Jeřáb, L. Peksa, J. Wild, F. Staněk, and M. Vičar. "Experimental study of gas flow through a multi-opening orifice." *Vacuum* 86, no. 11 (2012): 1759-1763. https://doi.org/10.1016/j.vacuum.2012.02.008

[6] Haimin, Wang, Xie Shujuan, Sai Qingyi, Zhou Caimin, Lin Hao, and Chen Eryun. "Experiment study on pressure drop of a multistage letdown orifice tube." *Nuclear Engineering and Design* 265 (2013): 633-638. https://doi.org/10.1016/j.nucengdes.2013.09.014

[7] Hollingshead, Colter L., Michael C. Johnson, Steven L. Barfuss, and Robert E. Spall. "Discharge coefficient performance of Venturi, standard concentric orifice plate, V-cone and wedge flow meters at low Reynolds numbers." *Journal of Petroleum Science and Engineering* 78, no. 3-4 (2011): 559-566. https://doi.org/10.1016/j.petrol.2011.08.008

[8] Martins, Nuno MC, Dídia IC Covas, Silvia Meniconi, Caterina Capponi, and Bruno Brunone. "Characterisation of low-Reynolds number flow through an orifice: CFD results vs. laboratory data." *Journal of Hydroinformatics* 23, no. 4 (2021): 709-723. https://doi.org/10.2166/hydro.2021.101

[9] Muñoz-Díaz, Enrique, Francisco J. Solorio-Ordaz, and Gabriel Ascanio. "A numerical study of an orifice flowmeter." *Flow Measurement and Instrumentation* 26 (2012): 85-92. https://doi.org/10.1016/j.flowmeasinst.2012.03.012

[10] Nygård, F., and H. I. Andersson. "Numerical simulation of turbulent pipe flow through an abrupt axisymmetric constriction." *Flow, Turbulence and Combustion* 91, no. 1 (2013): 1-18. https://doi.org/10.1007/s10494-013-9447-y

[11] Ramamurthi, Krishnaswami, and K. Nandakumar. "Characteristics of flow through small sharp-edged cylindrical orifices." *Flow measurement and Instrumentation* 10, no. 3 (1999): 133-143. https://doi.org/10.1016/S0955-5986(99)00005-9

[12] Rani, H. P., T. Divya, R. R. Sahaya, V. Kain, and D. K. Barua. "Numerical investigation of energy and Reynolds stress distribution for a turbulent flow in an orifice." *Engineering Failure Analysis* 34 (2013): 451-463. https://doi.org/10.1016/j.engfailanal.2013.08.010

[13] Karthik, G. S. Y., K. J. Kumar, and V. Seshadri. "Prediction of Performance Characteristics of Orifice Plate Assembly for Non-Standard Conditions Using CFD." *Int. J. Eng. Tech. Res* 3, no. 5 (2015): 162-167.

[14] Shaaban, S. "Optimization of orifice meter's energy consumption." *Chemical engineering research and design* 92, no. 6 (2014): 1005-1015. https://doi.org/10.1016/j.cherd.2013.08.022

[15] Shah, Manish S., Jyeshtharaj B. Joshi, Avtar S. Kalsi, C. S. R. Prasad, and Daya S. Shukla. "Analysis of flow through an orifice meter: CFD simulation." *Chemical Engineering Science* 71 (2012): 300-309. https://doi.org/10.1016/j.ces.2011.11.022

[16] Shan, Feng, Atsushi Fujishiro, Tatsuya Tsuneyoshi, and Yoshiyuki Tsuji. "Effects of flow field on the wall mass transfer rate behind a circular orifice in a round pipe." *International Journal of Heat and Mass Transfer* 73 (2014): 542-550. https://doi.org/10.1016/j.ijheatmasstransfer.2014.02.039

[17] Shih, Tsan-Hsing, William W. Liou, Aamir Shabbir, Zhigang Yang, and Jiang Zhu. "A new k-ϵ eddy viscosity model for high reynolds number turbulent flows." *Computers & Fluids* 24, no. 3 (1995): 227-238. https://doi.org/10.1016/0045-7930(94)00032-T

[18] Sridevi, T., Dhana Sekhar, and V. Subrahmanyam. "Comparison of Flow Analysis Through a Different Geometry of Flowmeters Using Fluent Software." *International Journal of Research in Engineering and Technology* 3, no. 08 (2014): 141-149. https://doi.org/10.15623/ijret.2014.0308023

[19] Vemulapalli, Sravani, and Santhosh Krishnan Venkata. "Parametric analysis of orifice plates on measurement of flow: A review." *Ain Shams Engineering Journal* 13, no. 3 (2022): 101639. https://doi.org/10.1016/j.asej.2021.11.008

[20] Zahariea, D. "Numerical analysis of eccentric orifice plate using ANSYS Fluent software." In *IOP Conference Series: Materials Science and Engineering*, vol. 161, no. 1, p. 012041. IOP Publishing, 2016. https://doi.org/10.1088/1757-899X/161/1/012041